



BIROn - Birkbeck Institutional Research Online

Crawford, Ian (2001) Ultra-high-resolution observations of interstellar Na I and K I towards the Scorpius OB1 association. *Monthly Notices of the Royal Astronomical Society* 328 (4), pp. 1115-1124. ISSN 0035-8711.

Downloaded from: <https://eprints.bbk.ac.uk/id/eprint/28524/>

Usage Guidelines:

Please refer to usage guidelines at <https://eprints.bbk.ac.uk/policies.html> or alternatively contact lib-eprints@bbk.ac.uk.

Ultra-high-resolution observations of interstellar Na I and K I towards the Scorpius OB1 association

I. A. Crawford[★]

Department of Physics and Astronomy, University College London, Gower Street, London WC1E 6BT

Accepted 2001 August 20. Received 2001 August 20; in original form 2001 July 9

ABSTRACT

I present ultra-high-resolution ($R \approx 9 \times 10^5$) observations of interstellar Na I and K I absorption lines towards three members of the Scorpius OB1 association (HD 152235, 152236 and 152249). These observations have, for the first time, resolved the intrinsic linewidths of most of the discrete absorption components present along these complex sightlines. The aims of the project were twofold: (i) to constrain the physical conditions prevailing in the highly blueshifted Sco OB1 shell components, and especially to search for evidence of active shocks within them; and (ii) to further constrain the low-velocity structure, where the Na I spectra are fully saturated but the unsaturated K I lines allow a clear resolution of the individual velocity components. The results of these analyses are discussed. Perhaps the most surprising result is the lack of any obvious correlation between the velocity dispersion of a velocity component (b -value) and its velocity. Specifically, the high-velocity shell components are generally found to be no broader than the low-velocity components attributed to foreground (often molecular) clouds, and cannot therefore be any hotter or more turbulent. Thus, with the possible exception of the most blueshifted component towards HD 152236, there is no evidence for active shocks in the shell components at present. However, consideration of the relative time-scales for post-shock cooling and grain surface adsorption indicates that shock processing in the past may still account for the low Na I/Ca II ratios of these components found in previous work.

Key words: shock waves – stars: individual: HD 152235 – stars: individual: HD 152236 – stars: individual: HD 152249 – ISM: structure – open clusters and associations: individual: Sco OB1.

1 INTRODUCTION

Many galactic OB associations are surrounded by expanding shells, many tens of parsecs in radius, driven by the cumulative effect of stellar winds and, in the more evolved cases, supernova explosions (e.g. Münch 1957; Cowie, Songaila & York 1979; Walborn 1982; Heiles 1984). The mechanical energy contained in these shells can have a profound effect on the structure of the interstellar medium in their vicinity, and, in extreme cases, the shells can break out of the galactic disc altogether, resulting in the ejection of the hot ionized material from their interiors into the galactic halo (Normandeau, Taylor & Dewdney 1996). In contrast to the situation in dense interstellar clouds, the heavy element abundances in these shells are not highly depleted, and this has been interpreted as being caused by the partial destruction of grains by shocks within them (Crawford, Barlow & Blades 1989 and references therein).

The Scorpius OB1 association ($l \approx 343^\circ$, $b \approx +1^\circ$) is situated in the Sagittarius spiral arm, ~ 1900 pc from the Sun (Humphreys 1978). It has an evolutionary age of $(3.8 \pm 0.6) \times 10^6$ yr (Raboud, Cramer & Bernasconi 1997; van Genderen, Bijleveld & van Groningen 1984), and contains one of the greatest concentrations of massive luminous stars known in the Galaxy. In earlier work (Crawford et al. 1989), we presented moderately high-resolution ($R \approx 10^5$) observations of interstellar Na I and Ca II absorption lines towards members of this OB association. These observations revealed a complex velocity structure, with strong (fully saturated in the case of Na I) absorption components close to zero heliocentric velocity (attributed to foreground interstellar clouds), and blueshifted components in the velocity range $-50 \lesssim v_{\text{helio}} \lesssim -20$ km s⁻¹ arising in the expanding Sco OB1 shell(s); a small number of redshifted absorption components were also identified. This earlier work found low Na I/Ca II column density ratios [$N(\text{Na I})/N(\text{Ca II}) \approx 1$] in the shell components, consistent with the removal of adsorbed Ca atoms from grain surfaces, and thus their return to the gas phase, by shock-induced sputtering. However, the

[★]E-mail: iac@star.ucl.ac.uk

resolving power of these earlier observations was insufficient to determine whether or not shocks are actually still present.

Here, I present observations of interstellar Na I and K I lines towards three Sco OB1 stars obtained at an order of magnitude higher resolution ($R \approx 9 \times 10^5$) using the Ultra High Resolution Facility (UHRF; see Diego et al. 1995) at the Anglo-Australian Telescope. Within the limits imposed by the signal-to-noise ratio, the UHRF is able to resolve the number of discrete absorption components present towards a given star down to the level of the intrinsic linewidths. This makes possible a much fuller understanding of the velocity structure along complicated lines of sight, and better constraints on the physical conditions from the line profiles, than is possible in lower resolution studies. The primary aims of this study were: (i) to search for evidence for the hypothesized shocks in the shell components, by placing limits on their thermal and turbulent properties; and (ii) to better constrain the low-velocity (foreground) structure through an analysis of the unsaturated K I line profiles.

2 OBSERVATIONS

Three Sco OB1 member stars, HD 152235, HD 152236 (ζ^1 Sco) and HD 152249 were observed, as listed in Table 1. A map showing the relative positions of these stars has been given by Crawford et al. (1989, their fig. 1), and a photograph of the region can be found on ESO Sky Survey Print B332. On the sky, these three stars form an almost straight line running north–south, with HD 152235 lying 22 arcmin due north of HD 152236 (the southernmost of the three), and HD 142249 lying 9 arcmin just east of north of HD 152235. At the estimated distance of the OB association, these angular separations correspond to 12 and 5 pc, respectively.

The 7698.974-Å line arising from K I was observed towards all three stars; the Na I D₁ (5895.924-Å) line was observed towards HD 152235 and 152249, while Na I D₂ (5889.951 Å) was observed towards HD 152236. With the exception of the latter observation [which was obtained with a 40- μ m-wide entrance slit during the UHRF commissioning observations in 1992 and an instrumental resolution of 0.42 km s⁻¹ FWHM; Barlow et al. (1995)], the spectrograph was used with a confocal image-slicer (Diego 1993), giving an average resolution of 0.345 ± 0.015 km s⁻¹ (measured using a stabilized He–Ne laser). The detector in 1992 was the AAO Thomson charge-coupled device (CCD)

(1024 × 1024 19- μ m pixels), while for all the other observations it was the AAO Tektronix CCD (1024 × 1024 24- μ m pixels). For the image-slicer observations, the CCD output was binned by a factor of 8 perpendicular to the dispersion direction in order to reduce the readout noise associated with the broad spectrum that results.

The spectra were extracted from the CCD images using the FIGARO data reduction package (Shortridge et al. 1998), and subsequent manipulations and measurements were performed using the DIPSO spectral analysis package (Howarth et al. 1998), at the UCL Starlink node. Scattered light was measured from the inter-order region and subtracted. Following this procedure, it was found that the flat cores of the strong interstellar Na D lines still lay above the nominal zero-level by between 2 and 5 per cent of the continuum intensity. As these line profiles indicate that they are indeed fully saturated, this additional background light level was also subtracted. No such independent check of the background intensity is possible for the non-saturated K I lines, and, for consistency, for a given star the same background correction was applied for the K I line as for the Na D line. Note that these minor background corrections have a negligible effect on the measured line widths, which are the main concern here. The spectra were then wavelength-calibrated using a Th–Ar comparison lamp. Telluric absorption lines occur in both spectral regions, and were removed by dividing each observed spectra by an atmospheric template obtained from observations of nearby, lightly reddened stars as described by Barlow et al. (1995). Finally, the spectra were converted to a heliocentric velocity scale and are shown in Fig. 1.

3 LINE-PROFILE ANALYSIS

The observed line profiles were modelled using a χ -squared minimization routine, VAPID (Howarth et al. 2001). This program returns the optimum values of column density (N), velocity dispersion (b) and central heliocentric velocity (v_{helio}) for a specified number of absorption components, and these values are given in Table 2. Both the Na I and K I lines exhibit hyperfine splitting (amounting to 1.08, 1.10 and 0.35 km s⁻¹ for Na D₁, Na D₂ and K I, respectively). This structure is fully resolved by the present observations in the case of Na I, and is comparable to the instrumental resolution in the case of K I. It must therefore be allowed for in the line-profile analysis, and the rest wavelengths

Table 1. List of observed stars and observational details. Spectral types are from the SIMBAD data base, and colour excesses ($E(B - V)$) are from van Genderen et al. (1984); S/N ratio is the continuum signal-to-noise ratio; $W\lambda(\text{tot})$ is the total equivalent width summed over all identified velocity components (2σ errors); and $\Delta v(\text{laser})$ is the measured FWHM of a stabilized He–Ne laser line, taken to indicate the spectral resolution.

Star (HD)	V	Sp.	$E(B - V)$	Line	UT date	Exps ($n \times s$)	S/N ratio	$W\lambda(\text{tot})$ (mÅ)	$\Delta v(\text{laser})$ (km s ⁻¹)
152235	6.4	B1 Iae	0.79	Na I D ₁	16-03-00	4 × 1800	80	629 ± 2	0.33 ± 0.01
				K I	31-07-99	9 × 1200 5 × 1800	53	173 ± 3	0.35 ± 0.01
152236	4.8	B1 Iape	0.69	Na I D ₂	15-07-92	3 × 1800	34	755 ± 5	0.42 ± 0.01
				K I	31-07-99	2 × 600	28	184 ± 4	0.35 ± 0.01
152249	6.5	O9 Ib	0.48	Na I D ₁	16-03-00	2 × 1800	31	692 ± 5	0.33 ± 0.01
				K I	21-04-00	3 × 1800	37	105 ± 4	0.36 ± 0.01

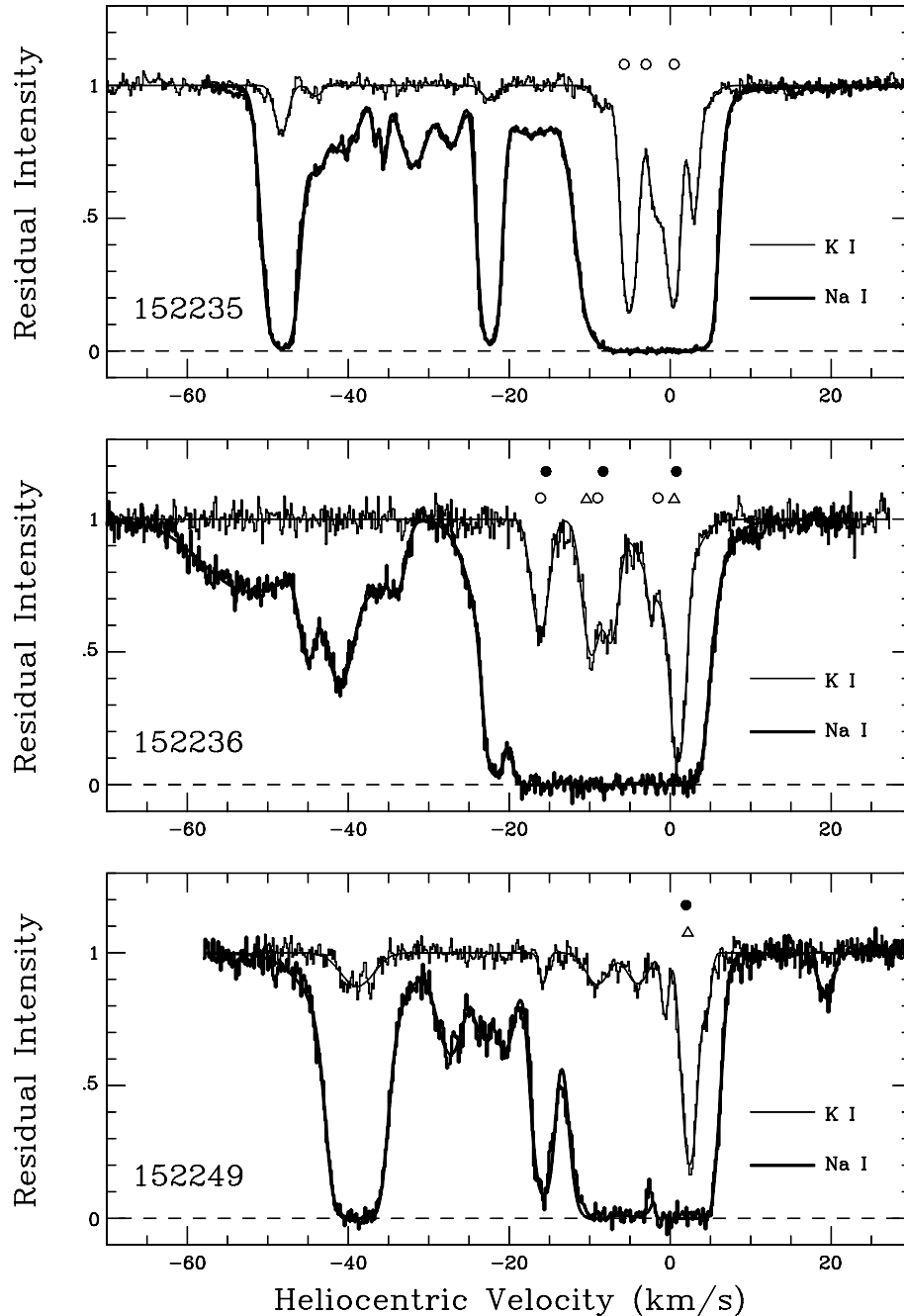


Figure 1. The interstellar Na I and K I lines towards the observed stars. The observed data are plotted as histograms, and the best-fitting theoretical line profiles (Table 2) are shown superimposed. Note that the small systematic velocity error noted in the text for K I has been corrected here (i.e. $0.3 \pm 0.1 \text{ km s}^{-1}$ has been added to the K I velocities). Solid circles indicate the velocities of the UV ($\lambda 3302$) Na I components identified by Crawford (1992). Open symbols indicate the velocities of *molecular* components identified by Crawford (1995, 1990, 1989) as follows: CH (open circles); CH and CN (open triangles; note that no CN observations were performed towards HD 152235, so this species may also be present towards this star).

and oscillator strengths of the individual hyperfine components of both species have been taken from Welty, Hobbs & Kulkarni (1994; their table A1). The quoted heliocentric velocities are with respect to the weighted mean central velocities of each hyperfine doublet as tabulated by Morton (1991). In the case of K I, I have neglected the very small (0.18 km s^{-1} ; e.g. Bendali, Duong & Vialle 1981) isotopic splitting between the ^{39}K and ^{41}K isotopes; ^{41}K contributes only 7 per cent to the terrestrial K abundance, and trial modelling indicated that its inclusion at this level has a negligible effect on the resulting line profiles. It is true, as pointed

out by the referee, that a significantly larger $^{41}\text{K}/^{39}\text{K}$ abundance ratio would both marginally broaden the lines (for a given b), and cause a slight ($\approx 0.18 \text{ km s}^{-1}$) shift of the line centre to shorter wavelengths. However, there seems to be no reason to expect an anomalous $^{41}\text{K}/^{39}\text{K}$ ratio in the interstellar medium in general, or the Sco OB1 components in particular – for example, the summary of nucleosynthetic products of type II and Ia supernovae given by Iwamoto et al. (1999; their table 3) indicates an essentially terrestrial $^{41}\text{K}/^{39}\text{K}$ ratio.

A glance at the best-fitting velocities of well-defined

Table 2. The best-fitting line-profile parameters (with 1σ errors). Asterisks indicate Na I components within the saturated region (see Fig. 1), with velocities tied to the identified K I components (allowing for the small systematic velocity shifts discussed in Section 3); as discussed in the text, it is likely that additional Na I components, too weak to be detected in K I, also exist in this velocity range. For components not identified in K I, the column density upper limits are 3σ values (based on the continuum signal-to-noise ratio, the width of the corresponding Na I component, and a linear curve of growth). R_{NaK} is the Na I/K I column density ratio; values in parentheses are uncertain, and perhaps meaningless, owing to the probable presence of additional unrecognized Na I components.

Star (HD)	Na I			K I			R_{NaK}
	v_{helio} (km s^{-1})	b (km s^{-1})	$\log N$ (cm^{-2})	v_{helio} (km s^{-1})	b (km s^{-1})	$\log N$ (cm^{-2})	
152235	-48.31 ± 0.02	1.73 ± 0.02	12.49 ± 0.01	-48.55 ± 0.04	1.05 ± 0.06	10.75 ± 0.02	55^{+4}_{-4}
	-44.08 ± 0.12	1.15 ± 0.26	11.21 ± 0.11	-44.30 ± 0.18	0.94 ± 0.26	10.02 ± 0.09	16^{+9}_{-6}
	-40.71 ± 0.32	2.64 ± 0.45	11.44 ± 0.07	–	–	≤ 9.99	≥ 24
	-35.95 ± 0.05	0.51 ± 0.06	10.98 ± 0.04	–	–	≤ 9.64	≥ 20
	-31.87 ± 0.09	2.22 ± 0.18	11.48 ± 0.02	–	–	≤ 9.95	≥ 32
	-27.27 ± 0.11	1.35 ± 0.20	11.15 ± 0.05	–	–	≤ 9.84	≥ 18
	-22.43 ± 0.01	1.03 ± 0.03	12.23 ± 0.01	-22.66 ± 0.14	1.15 ± 0.21	10.24 ± 0.06	98^{+17}_{-15}
	-17.30 ± 0.37	5.03 ± 1.16	11.56 ± 0.08	–	–	≤ 10.13	≥ 22
	-8.49^*	2.61 ± 0.07	12.52 ± 0.01	-8.71 ± 0.10	1.21 ± 0.16	10.45 ± 0.04	(118^{+14}_{-13})
	-5.08^*	1.67 ± 0.24	13.02 ± 0.18	-5.30 ± 0.01	1.10 ± 0.01	11.75 ± 0.01	(19^{+10}_{-7})
	-1.17^*	1.54 ± 1.80	12.62 ± 0.25	-1.83 ± 0.07	1.33 ± 0.08	11.38 ± 0.03	(17^{+16}_{-8})
	$+0.43^*$	0.93 ± 0.08	14.42 ± 0.25	$+0.21 \pm 0.02$	0.93 ± 0.03	11.64 ± 0.02	(600^{+500}_{-300})
	$+2.91^*$	2.90 ± 1.29	11.66 ± 0.64	$+2.69 \pm 0.03$	0.72 ± 0.09	11.10 ± 0.12	(4^{+17}_{-3})
$+3.88^*$	1.36 ± 0.06	12.41 ± 0.07	$+3.66 \pm 1.53$	1.75 ± 1.03	10.61 ± 0.50	(63^{+170}_{-46})	
152236	-51.88 ± 0.43	8.16 ± 0.60	11.67 ± 0.03	–	–	≤ 10.51	≥ 13
	-45.01 ± 0.12	1.12 ± 0.20	11.12 ± 0.08	–	–	≤ 10.08	≥ 9
	-41.00 ± 0.36	2.19 ± 0.51	11.57 ± 0.13	–	–	≤ 10.22	≥ 17
	-36.59 ± 0.84	2.31 ± 3.48	11.10 ± 0.69	–	–	≤ 10.23	≥ 2
	-33.81 ± 0.47	1.12 ± 0.92	10.77 ± 0.78	–	–	≤ 10.08	≥ 1
	-21.83 ± 0.06	0.92 ± 0.19	11.71 ± 0.13	–	–	≤ 10.04	≥ 35
	-18.53 ± 0.75	4.84 ± 1.33	12.16 ± 0.62	–	–	≤ 10.40	≥ 14
	-16.17^*	1.76 ± 0.82	12.87 ± 0.31	-16.47 ± 0.05	1.33 ± 0.07	11.29 ± 0.02	(38^{+43}_{-20})
	-9.80^*	2.59 ± 0.97	12.56 ± 0.26	-10.10 ± 0.11	1.39 ± 0.12	11.41 ± 0.04	(14^{+14}_{-7})
	-7.33^*	3.99 ± 2.02	12.60 ± 0.30	-7.63 ± 0.11	1.18 ± 0.14	11.26 ± 0.06	(22^{+28}_{-12})
	-2.46^*	6.26 ± 2.99	12.11 ± 1.29	-2.76 ± 0.09	0.24 ± 0.22	10.31 ± 0.14	(63^{+1600}_{-61})
	-0.44^*	3.41 ± 1.31	12.36 ± 0.81	-0.74 ± 0.17	3.55 ± 0.20	11.57 ± 0.03	(6^{+36}_{-5})
$+0.96^*$	2.17 ± 0.42	12.48 ± 0.18	$+0.66 \pm 0.02$	0.91 ± 0.03	11.72 ± 0.02	(6^{+3}_{-2})	
152249	-39.02 ± 0.33	6.38 ± 1.05	11.96 ± 0.10	–	–	≤ 10.33	≥ 34
	-38.92 ± 0.03	2.33 ± 0.10	12.90 ± 0.03	-39.32 ± 0.16	2.74 ± 0.23	10.98 ± 0.03	83^{+12}_{-11}
	-27.24 ± 0.16	2.07 ± 0.29	11.57 ± 0.05	–	–	≤ 10.09	≥ 27
	-23.43 ± 0.28	0.96 ± 0.48	11.17 ± 0.18	–	–	≤ 9.92	≥ 12
	-20.60 ± 0.27	1.57 ± 0.43	11.46 ± 0.09	–	–	≤ 10.03	≥ 22
	-15.78 ± 0.03	1.26 ± 0.06	12.11 ± 0.01	-16.21 ± 0.09	0.59 ± 0.14	10.32 ± 0.07	62^{+13}_{-10}
	-9.06^*	2.44 ± 0.06	12.81 ± 0.02	-9.49 ± 0.15	1.86 ± 0.23	10.79 ± 0.04	(110^{+16}_{-14})
	-4.05^*	2.32 ± 0.21	12.63 ± 0.03	-4.48 ± 0.16	1.76 ± 0.26	10.75 ± 0.05	(76^{+15}_{-14})
	-0.67^*	0.26 ± 0.29	13.10 ± 2.85	-1.10 ± 0.04	0.52 ± 0.07	10.63 ± 0.04	$(300^{+\infty}_{-300})$
	$+2.40^*$	1.14 ± 0.38	13.64 ± 0.83	$+1.97 \pm 0.02$	1.07 ± 0.02	11.66 ± 0.01	(96^{+570}_{-82})
	$+4.56^*$	1.38 ± 0.17	12.10 ± 0.07	$+4.13 \pm 0.06$	0.59 ± 0.10	10.61 ± 0.05	(31^{+10}_{-8})
$+19.30 \pm 0.18$	0.81 ± 0.32	10.90 ± 0.08	–	–	≤ 9.89	≥ 9	

components measured in both Na I and K I (Table 2) suggests the presence of a small systematic velocity calibration difference between these two species. Specifically, we find that the K I velocities are systematically lower than the Na I velocities, by $\approx 0.22 \text{ km s}^{-1}$ for HD 152235 and 0.43 km s^{-1} for HD 152249; as no well-defined narrow components were observed in K I towards HD 152236, a similar comparison was not possible in this case. An essentially identical velocity shift ($v_{\text{NaI}} - v_{\text{KI}} = 0.30 \pm 0.10 \text{ km s}^{-1}$) is present in the extensive UHRF observations of

interstellar lines towards Orion presented by Price et al. (2001). Comparison with UHRF velocities measured for other species (e.g. Ca II, Price et al. 2001) confirm that it is the K I velocities that are discrepant. The origin of this small systematic velocity shift is currently unknown and is under investigation. It would translate to a $\sim 8 \text{ m\AA}$ error in the rest wavelength of the K I resonance line, which seems implausibly large (although it is of the same order, and in the correct sense, as the $^{39}\text{K}/^{41}\text{K}$ isotope shift, resorting to this explanation would imply an anomalous isotope ratio as

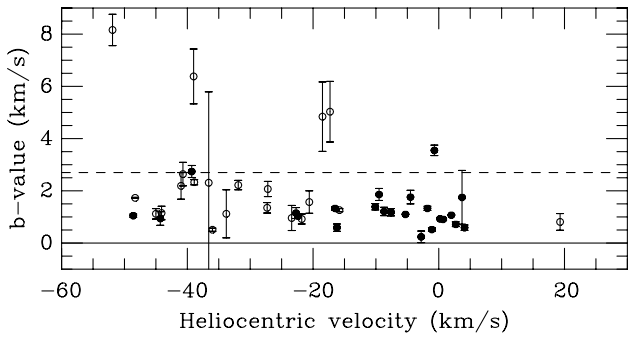


Figure 2. The measured b -values as a function of radial velocity for the Sco OB1 absorption components. Filled circles indicate K I and open circles indicate Na I. The horizontal dashed line at $b = 2.7 \text{ km s}^{-1}$ corresponds to thermal broadening for Na at $T_k = 10^4 \text{ K}$, as expected behind a 20 km s^{-1} shock (see text); the corresponding b -value for K is 2.1 km s^{-1} . It is clear that most of these components are formed in much cooler gas; the weighted mean b -value ($1.15 \pm 0.01 \text{ km s}^{-1}$) corresponds to a temperature upper limit of 1800 K for Na I (3100 K for K I).

discussed above). Much more likely is a calibration error resulting from wavelength errors in the small number (typically four) Th–Ar comparison lines found within the restricted ($\approx 4 \text{ \AA}$) coverage of the detector at this resolution. Whatever the explanation, the Na I velocities listed in Table 2 should be taken as the ‘true’ heliocentric velocities of the various absorption components.

Fig. 1 clearly reveals that the velocity range occupied by the broad, fully saturated, Na I absorption troughs actually contains several discrete absorption components, as traced by the unsaturated K I lines. It is of interest to determine whether the fully saturated Na I line profiles can be modelled by assuming the velocity structure observed in K I, or whether additional Na I components are required. Thus, over the velocity range occupied by fully saturated absorption, the Na I line-profile fits were performed on the basis of discrete absorption components with velocities fixed at the K I values (after allowing for the systematic velocity shift discussed above), but allowing the b and N values to remain free parameters. These Na I components are indicated by asterisks in Table 2. It can be seen that this restriction does indeed result in acceptable fits to the fully saturated regions of the Na I spectra, although the fact that some of the resulting Na I b -values are much broader than the well-defined K I components strongly suggests that, in fact, additional Na I components are also present in this velocity range.

Finally, I note that the line-profile modelling routine has implicitly assumed Voigt profiles, and hence a Gaussian distribution of velocities for the individual absorbers contributing to each velocity component. The referee has drawn attention to the possibility that non-Gaussian velocity distributions might be expected in post-shock environments, such as those discussed below. While it is important to bear this possibility in mind, I note that all of the well-resolved components observed here are well-fitted on the assumption of Voigt profiles, and that there is therefore no compelling evidence in the present data for non-Gaussian velocity distributions within discrete absorption components.

4 THE LINEWIDTHS

The main interest of the present work is in the intrinsic linewidths, as here these have been resolved by the UHRF for the first time, and may be used to constrain the physical conditions in the

absorbing media. The velocity dispersion parameters (b -values) are given in Table 2, and are related to the full width at half maximum (FWHM) of the line profiles by $\text{FWHM} = 1.6651 \times b$. Fig. 2 plots the measured b -values as a function of heliocentric velocity, and shows that most of the components are quite narrow, with $b \lesssim 2 \text{ km s}^{-1}$. In the case of the well-defined K I components, the weighted mean b -value is $1.07 \pm 0.01 \text{ km s}^{-1}$, within the range found by Welty & Hobbs (2001) in their extensive survey of interstellar K I lines, but broader than their median value of 0.67 km s^{-1} . Interestingly, there is no significant dependence of b -value on velocity, the significance of which we discuss below.

We note that some of these features may actually be unresolved blends of still narrower components. The clearest example is the -38.92 km s^{-1} component ($b_{\text{Na I}} = 2.33 \pm 0.10 \text{ km s}^{-1}$) towards HD 152249. Although saturated in Na I, the unsaturated K I profile is consistent with the presence of two narrower components, even though the signal-to-noise ratio of the present data is not sufficient to demonstrate this. Clearly, if such substructure is present then the b -values of each will be narrower, placing still tighter constraints on the physical conditions discussed below. The small number of very broad, generally Na I, components ($b \gtrsim 4 \text{ km s}^{-1}$), can also generally be explained by unrecognized blends of additional velocity structure (although there is a possible exception in the -51.9 km s^{-1} component towards HD 152236, discussed further in Section 6.2).

The primary line-broadening mechanisms in the neutral interstellar medium are thermal Doppler broadening, and broadening owing to bulk motions of the gas (‘turbulence’). These combine to produce an observed velocity dispersion, b , as follows:

$$b = \sqrt{\frac{2kT_k}{m_A} + 2v_t^2}, \quad (1)$$

where T_k is the kinetic temperature, v_t is the line-of-sight turbulent velocity, k is Boltzmann’s constant and m_A is the mass of the element (of atomic mass A) under observation.

Equation (1) can be used to place constraints on the physical conditions in several ways. First, by solving for a measured b -value, and setting $v_t = 0$, we may obtain a rigorous upper limit, T_k^{ul} , for the kinetic temperature in that absorption component. Similarly, by setting $T_k = 0$ we may obtain a rigorous upper limit to the line-of-sight turbulent velocity, v_t^{ul} . These upper limits (based on the upper limits quoted on the measured b -values) are listed in Table 3 for all the absorption components identified here. Since we expect all components to have a non-zero temperature, and to be turbulent to some extent, the actual values of both quantities must lie below these upper limits.

Finally, if the same absorption component is identified in two species having a significant mass difference, and if it is assumed that both species co-exist spatially in a given absorption component, then equation (1) may be solved to obtain both T_k and v_t simultaneously. These conditions are satisfied for Na I ($A = 23$) and K I ($A = 39$), where the similar ionization potentials (5.1 and 4.3 eV , respectively) and grain adsorption binding energies (Barlow 1978), lead us to expect that both species will indeed occur co-spatially. Note that, for these assumptions, physically meaningful solutions must lie in the range $1.0 \leq b(\text{Na I})/b(\text{K I}) \leq 1.30$ (i.e. the range between purely turbulent broadening on the one hand, and purely thermal broadening on the other). If this condition is not met [generally because $b(\text{Na}) > 1.30 \times b(\text{K})$; Table 2], the most likely reason is that additional unrecognized velocity structure is present.

Table 3. The kinetic temperature and turbulence upper limits (T_K^{ul} and v_t^{ul} , respectively) for absorption components identified towards Sco OB1. So that they may be considered rigorous upper limits, these values are based on the (1σ) upper limits to the b -values given in Table 2. Where a simultaneous solution of equation (1) (including the errors on the Na I and K I b -values) proved possible, the range of allowed solutions for T_k and v_t is given in the last two columns.

Star (HD)	v_{helio} (km s $^{-1}$)	T_K^{ul} (K)	T_K^{ul} (K)	v_t^{ul} (Na) (km s $^{-1}$)	v_t^{ul} (K) (km s $^{-1}$)	T_k range (K)	v_t range (km s $^{-1}$)
152235	-48.31	4 240	2 890	1.24	0.78	No soln	No soln
	-44.08	2 750	3 380	1.00	0.85	0.00–2750	0.00–0.85
	-40.71	13 210	–	2.18	–	–	–
	-35.95	450	–	0.40	–	–	–
	-31.87	7 970	–	1.70	–	–	–
	-27.27	3 320	–	1.10	–	–	–
	-22.43	1 550	4 340	0.75	0.96	0.00–810	0.52–0.75
	-17.30	53 000	–	4.38	–	–	–
	-8.49	9 940	4 400	1.90	0.97	No soln	No soln
	-5.08	5 050	2 890	1.35	0.78	2740–2890	0.00–0.18
	-1.17	15 400	4 660	2.36	1.00	0.00–4660	0.00–1.00
	+0.43	1 410	2 160	0.71	0.68	0.00–708	0.51–0.68
	+2.91	24 300	1 540	2.96	0.57	No soln	No soln
	+3.88	2 790	18 100	1.00	1.97	0.00–2790	0.00–1.00
152236	-51.88	106 000	–	6.19	–	–	–
	-45.01	2 410	–	0.93	–	–	–
	-41.00	10 100	–	1.91	–	–	–
	-36.59	46 400	–	4.09	–	–	–
	-33.81	5 760	–	1.44	–	–	–
	-21.83	1 700	–	0.78	–	–	–
	-18.53	52 700	–	4.36	–	–	–
	-16.17	9 210	4 600	1.82	0.99	0.00–4600	0.00–0.99
	-9.80	17 500	5 350	2.52	1.07	1160–5350	0.00–0.94
	-7.33	50 000	4 090	4.25	0.93	No soln	No soln
	-2.46	118 000	500	6.54	0.33	No soln	No soln
	-0.44	30 800	33 000	3.34	2.65	0.00–30800	0.00–2.65
+0.96	9 280	2 070	1.83	0.66	No soln	No soln	
152249	-39.02	76 400	–	6.19	–	–	–
	-38.92	8 170	20 700	1.72	2.10	No soln	No soln
	-27.24	7 700	–	1.67	–	–	–
	-23.43	2 870	–	1.02	–	–	–
	-20.60	5 530	–	1.41	–	–	–
	-15.78	2 410	1 250	0.93	0.52	No soln	No soln
	-9.06	8 640	10 200	1.77	1.48	4370–8640	0.00–1.12
	-4.05	8 850	9 570	1.79	1.43	1250–8850	0.00–1.33
	-0.67	420	820	0.39	0.42	0.00–340	0.17–0.39
	+2.40	3 200	2 790	1.07	0.77	0.00–2790	0.00–0.77
	+4.56	3 320	1 120	1.10	0.49	No soln	No soln
	+19.30	1 770	–	0.80	–	–	–

5 THE Na I/K I RATIOS

Although the b -values were the main focus of the present work, Welty & Hobbs (2001) have drawn attention to potentially interesting information contained in the Na I/K I ratio, R_{NaK} , and a brief discussion is appropriate. The values of R_{NaK} found for the components identified here are listed in the last column of Table 2. However, an immediate word of caution is required regarding those within the velocity range occupied by fully saturated Na I: the probable presence of additional, unidentified, Na I components renders these ratios uncertain at best, and perhaps meaningless; they are listed in parentheses in Table 2 to indicate this uncertainty. Only those R_{NaK} values deduced from components clearly resolved in both species can be used to say anything meaningful concerning the prevailing physical conditions. Unfortunately, excluding the upper limits, there are only five such values (unbracketed in Table 2), all corresponding to the relatively high velocity shell components. Of these, four lie in the range $55 \lesssim R_{\text{NaK}} \lesssim 98$ (with a mean value of 74.5), while one (the weak -44.08 km s $^{-1}$

component towards HD 152235) has the much lower value of $R_{\text{NaK}} \approx 16$.

From their high-resolution study of 54 stars, Welty & Hobbs (2001) found a median R_{NaK} value of about 85, although in the relatively low column density regime appropriate here [$\log N(\text{K I}) \approx 10.50$] their best data (33 stars; cf. their table 2) yields the slightly lower value of $R_{\text{NaK}} \approx 74$. This is close to the average value obtained here, and is in good agreement with the value expected for photoionization equilibrium in a low-density gas immersed in a ‘standard’ interstellar radiation field. For example, taking the photoionization and recombination rates from Péquignot & Aldrovandi (1986), and other assumptions as given in section 4 of Crawford et al. (2000), we obtain $R_{\text{NaK}} = 71$ for $n_{\text{H}} = 10 \text{ cm}^{-3}$ and $T_k = 100$ K. Higher densities and, to a lesser extent, lower temperatures decrease R_{NaK} ; for example, the same assumptions yield $R_{\text{NaK}} = 49$ for $n_{\text{H}} = 1000 \text{ cm}^{-3}$ and $T_k = 10$ K.

As noted by Welty & Hobbs (2001), R_{NaK} exhibits wide variations, both towards different areas of sky (for example, for reasons that are currently not understood it is about a factor of 2

lower than ‘normal’ towards stars in Sco-Oph), and between different components towards a given star (values of 86 and 42 being found by Welty & Hobbs for two discrete components towards 1 Sco). With the exception of the anomalous -44.08 km s^{-1} component towards HD 152235, this range of variability is generally consistent with the present results for the Sco OB1 components. Possible reasons for variation in R_{NaK} are discussed at length by Welty & Hobbs (2001), who note that changes in the strength or spectrum of the ambient radiation field are unlikely to be responsible. The simple photoionization calculation given above suggests that variations in density, and/or H ionization fraction, may be at least partly responsible. It is interesting to note that while a very high density ($n_{\text{H}} \approx 1000 \text{ cm}^{-3}$) would be required to account for the low ($R_{\text{NaK}} \approx 55$) value found for the most blueshifted ($v_{\text{helio}} = -48.31 \text{ km s}^{-1}$) component towards HD 152235 under the assumption that hydrogen is neutral, a modest hydrogen ionization fraction ($n_{\text{e}}/n_{\text{H}} = 0.1$) yields $R_{\text{NaK}} \approx 55$ for $n_{\text{H}} = 10 \text{ cm}^{-3}$ and $T_{\text{k}} = 100 \text{ K}$. The very low value found for the -44.08 km s^{-1} component towards HD 152235 ($R_{\text{NaK}} \approx 16$) seems difficult to reconcile with any of the proposed explanations, and further study may be warranted.

6 DISCUSSION

As discussed by Crawford et al. (1989), the Sco OB1 absorption components fall naturally into three categories: those that are blueshifted with respect to the radial velocity of the OB association, and therefore most likely arise in the expanding shell(s) surrounding it; those that occur at lower velocities (generally fully saturated in Na I) and which probably arise in foreground clouds; and those (only one in the present sample) which occur at significant positive radial velocities. Following a brief discussion of the radial velocity of Sco OB1 itself, we will discuss the various components observed here according to these groupings.

6.1 The Sco OB1 radial velocity

Recently, Dambis, Mel’nik & Rastorguev (2001) have determined the Sco OB1 heliocentric radial velocity to be $-27.6 \pm 2.2 \text{ km s}^{-1}$ (this being the median value for 26 member stars). This very recent value is in generally good agreement with the earlier published values of $-29.1 \pm 2.4 \text{ km s}^{-1}$ (Struve 1944) and $-23.9 \pm 1.4 \text{ km s}^{-1}$ (Laval 1972). These values may be compared with that expected from galactic rotation, although unfortunately the distance of Sco OB1 is still somewhat uncertain. The canonical value is 1900 pc (Humphreys 1978), although Dambis et al. have argued that all of Humphrey’s OB association distances are overestimated by ~ 10 per cent, which would imply a distance of $\sim 1700 \text{ pc}$ for Sco OB1. This is in good agreement with a recent photometric study of the central cluster of Sco OB1 (NGC 6231) by Raboud et al. (1997), who obtained a distance of $1757 \pm 370 \text{ pc}$. On the other hand, the exhaustive analysis of Perry, Hill & Christodoulou (1991) yielded a value of 2000 pc. If we adopt a distance of $1900_{-200}^{+100} \text{ pc}$, the galactic rotation model of Fich, Blitz & Stark (1989) leads to expect a radial velocity of $-22_{-1}^{+2} \text{ km s}^{-1}$. This is in generally good agreement with the measured values, especially that of Laval (1972).

On the basis of this discussion, and the general morphology of the spectra (Fig. 1), here we will consider components with radial velocities more negative than -20 km s^{-1} to arise in shells

surrounding the OB association. However, we recognize that the precise radial velocity boundary between these and foreground clouds unrelated to Sco OB1 is uncertain at the several km s^{-1} level. In this direction, zero velocity with respect to the local standard of rest (LSR) is $\approx +6 \text{ km s}^{-1}$ heliocentric, so heliocentric velocities in the range -20 to $+6 \text{ km s}^{-1}$ are consistent with foreground material corotating with the galaxy.

6.2 The shell components

Perhaps the most noteworthy feature of the Sco OB1 shell components is that, with a few exceptions, they are not significantly broader (and therefore not significantly hotter or more turbulent) than those arising in the low-velocity foreground clouds (Fig. 2). Given the evidence for the shock processing of grains in these components (Crawford et al. 1989) this was an unexpected result. The work of Barlow & Silk (1977) and Barlow (1978) indicates that shock velocities of $\geq 20 \text{ km s}^{-1}$ are required for the effective removal of adsorbed Ca atoms from grain surfaces, as invoked by Crawford et al. (1989) to account for the low Na I/Ca II ratios observed in these components. Although modest by many interstellar standards, such a shock velocity would still result in post-shock kinetic temperatures $\geq 10^4 \text{ K}$ for a neutral atomic gas containing 10 per cent He by number (e.g. McKee & Hollenbach 1980, their equation 8). In the absence of turbulence, this corresponds to a Na *b*-value of 2.7 km s^{-1} (dashed line in Fig. 2), and it is clear that most of the observed shell components are significantly narrower than this. Put another way, the rigorous upper limits to the temperature, T_{k}^{ul} (Table 3) are generally lower than the *minimum* expected post-shock temperatures. The most extreme example is the -35.95 km s^{-1} component towards HD 152235, for which the hyperfine structure of Na I is clearly resolved (Fig. 1) and for which the well-defined *b*-value ($0.51 \pm 0.06 \text{ km s}^{-1}$) implies a rigorous upper limit to T_{k} of only 450 K.

It appears, however, that the general absence of hot gas in these components is not necessarily inconsistent with the shock removal of adsorbed Ca from grain surfaces invoked by Crawford et al. (1989). McKee & Hollenbach [1980; their equation (11), noting that $t_{\text{cool}} = N_{\text{cool}}/n_{\text{H}}v_{\text{s}}$, where N_{cool} is the column density of cooling gas] give the characteristic post-shock cooling time, t_{cool} , for shock velocities in the appropriate range ($20 \lesssim v_{\text{s}} \lesssim 60 \text{ km s}^{-1}$) as

$$t_{\text{cool}} \approx \frac{2.0 \times 10^{11} \times v_{\text{s}}^{-5}}{n_{\text{H}}} \text{ yr}, \quad (2)$$

where n_{H} is the pre-shock density (cm^{-3}) and v_{s} is in km s^{-1} . Thus for $v_{\text{s}} = 20 \text{ km s}^{-1}$ and $n_{\text{H}} = 10 \text{ cm}^{-3}$ we have $t_{\text{cool}} \approx 6300 \text{ yr}$. We obtain essentially the same order of magnitude for t_{cool} ($\approx 10^4 \text{ yr}$) using the canonical expression for warm H I gas given by Spitzer (1978, p. 142), and we note that the cooling time will be even shorter for hotter and/or higher-density gas.

On the other hand, following Barlow (1978), we may estimate the depletion time-scale for a particular species, t_{dep} , as its number density divided by the rate (per unit volume) at which atoms of that species encounter interstellar grains (note that this is actually a lower limit to the depletion time-scale as it implicitly assumes a sticking probability of unity). This yields $t_{\text{dep}} \sim 1/\Sigma_{\text{d}}v$, where Σ_{d} is the mean grain cross-sectional area per unit volume, and v is the velocity of the atom relative to the grains. Spitzer (1978, p. 162) gives $\Sigma_{\text{d}} \approx 1.0 \times 10^{-21} n_{\text{H}} \text{ cm}^{-1}$. Adopting this, and assuming the

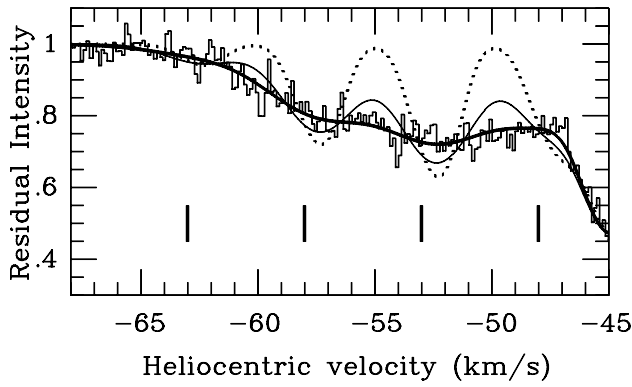


Figure 3. An expanded view of the Na I spectrum of HD 152236, in the region of the broad -51.88 km s^{-1} component. Here, it has been modelled by four narrower subcomponents (at the velocities indicated by the vertical tick marks), each with freely varying column densities but with b -values fixed at 1 km s^{-1} (dotted line); 2 km s^{-1} (light solid line); and 3 km s^{-1} (heavy solid line). Clearly, only the latter solution would have gone undetected in the present data. See the text for a discussion.

grain velocity is purely thermal, we obtain:

$$t_{\text{dep}} \approx \frac{2.5 \times 10^9 \times \sqrt{A}}{n_{\text{H}} \times \sqrt{T_{\text{k}}}} \text{yr.} \quad (3)$$

For Ca ($A = 40$) at $T_{\text{k}} = 10^4 \text{ K}$, and $n_{\text{H}} = 10 \text{ cm}^{-3}$ as above, we find $t_{\text{dep}} \approx 1.6 \times 10^7 \text{ yr}$. This is not only three orders of magnitude longer than the post-shock cooling time, but is an order of magnitude longer than the age of Sco OB1 itself! Thus, we conclude that the Sco OB1 shell components may indeed have had their Ca atoms removed from grain surfaces by shock processing in the past. While the gas has long since cooled, there has been insufficient time for sputtered atoms to have been re-adsorbed on to the grains.

There are a handful of broader components, all identified in Na I. Excluding the poorly defined components within the fully saturated Na I velocity range (marked with asterisks in Table 2), the most notable of these are the -17.3 km s^{-1} component towards HD 152235 ($b = 5.03 \pm 1.16 \text{ km s}^{-1}$), the -51.9 and -18.5 km s^{-1} components towards HD 152236 ($b = 8.16 \pm 0.60$ and $4.84 \pm 1.33 \text{ km s}^{-1}$, respectively), and the -39.0 km s^{-1} component towards HD 152249 ($b = 6.38 \pm 1.05 \text{ km s}^{-1}$). Most of these components are quite poorly defined (as indicated by the large errors) and can most plausibly be accounted for by the presence of additional velocity structure, which is not resolved at the signal-to-noise ratio of the present data.

However, the very broad, and seemingly well defined, -51.9 km s^{-1} component towards HD 152236 is worthy of further discussion. It turns out that, at the resolution employed here, it is not easy to hide additional velocity structure within the profile of this component. Indeed, as we might expect, this can only plausibly be achieved by postulating a number of subcomponents with velocity separations less than or approximately equal to their FWHM ($1.6651b$). We illustrate this in Fig. 3. The apparently unblended region of the -51.9 component occupies the velocity range $-63 \lesssim v_{\text{helio}} \lesssim -48 \text{ km s}^{-1}$. In Fig. 3 we have replaced the original -51.9 component by four subcomponents within this range, each separated by 5 km s^{-1} . The column density of each was left as a free parameter, and three separate fits were performed for $b = 1, 2$ and 3 km s^{-1} . As can be seen, any such structure would have been resolved for $b \lesssim 3 \text{ km s}^{-1}$ (FWHM $\lesssim 5 \text{ km s}^{-1}$). For

$b \approx 1 \text{ km s}^{-1}$, approximately nine such discrete subcomponents would be required.

Although we cannot absolutely exclude such substructure, there is a real possibility that, unlike all of the other well-defined shell components, the -51.9 component towards HD 152236 does arise in a very hot and/or turbulent medium. Such hot and/or turbulent conditions may imply that this component arises in a recently swept-up and/or ejected structure, consistent with it being the highest-velocity component present towards this star. Its absence towards HD 152235 (22 arcmin to the north) implies a linear dimension of $\lesssim 12 \text{ pc}$, and it may well be local to HD 152236 itself [which we note is by far the most luminous member of the Sco OB1 association, and, in fact, is one of the most luminous stars known in the Galaxy; e.g. Humphreys (1978)].

6.3 The foreground components

The presence of unresolved velocity structure within the broad Na I absorption troughs near zero heliocentric velocity was apparent from the Ca II absorption-line profiles presented by Crawford et al. (1989). Subsequently, the low-velocity Na I velocity structure towards two of these stars (HD 152236 and 152249) was studied at $R = 50\,000$ (6 km s^{-1} FWHM) resolution using the unsaturated ultraviolet ($\lambda 3302$) Na I doublet (Crawford 1992a). The velocities of these components are indicated in Fig. 1 (filled circles). As we would expect, there is good agreement between the ultraviolet (UV) Na I and K I velocities, although the present observations indicate that additional velocity structure is present that was below the resolution of the earlier study. Relatively high densities ($n_{\text{H}} \approx 10^2 \text{ cm}^{-3}$) are indicated for these components by the large Na I/Ca II ratios ($\approx 10^2$), resulting from the adsorption of most of the available gas-phase Ca on to grain surfaces (Crawford 1992a and references therein). Observations of simple diatomic molecules (CH, CH⁺ and CN) have been obtained towards all three stars (Crawford 1989, 1990, 1995). The velocities of the molecular components are also indicated in Fig. 1 (open symbols). Again, there is good agreement between the molecular and K I components, indicating that the latter trace the densest, at least partly molecular, material. The close association between K I and molecular (CH) gas has also been noted by Welty & Hobbs (2001); but see below for a caveat.

As discussed in Section 6.1, velocity components in the range $-20 \lesssim v_{\text{helio}} \lesssim +6 \text{ km s}^{-1}$ are consistent with galactic rotation over the ~ 1900 -pc line of sight. Thus, most of these components presumably arise in foreground clouds unrelated to Sco OB1. For the purpose of discussion, these components may be conveniently divided between those thought to arise in relatively nearby ($\approx 150 \text{ pc}$) molecular gas, and those that arise in more distant clouds.

6.3.1 The molecular components

As discussed by Crawford (1992b, section 4.7) components in the velocity range $-6 \lesssim v_{\text{helio}} \lesssim +6 \text{ km s}^{-1}$, which includes all of the strongest K I components observed here, most plausibly arise in outlying gas associated with the Lupus molecular cloud complex at a distance of $\approx 150 \text{ pc}$ (e.g. Crawford 2000). Within this velocity range, the absorption-line profiles of HD 152236 and 152249 are quite similar, while HD 152235 exhibits more complex structure (Fig. 1). This is especially interesting, as HD 152235 lies *between* the other two stars as seen on the sky. If all of this structure does indeed arise at the Lupus distance of 150 pc , it implies significant

inhomogeneities on a scale of 0.4 pc or less (corresponding to the 9-arcmin separation of HD 152235 and 152249). It is true that if these additional low-velocity components arise beyond the Lupus clouds, the spatial scale of this structure would be increased, but it cannot exceed 5 pc (the separation of the lines of sight at the stellar distances). We note that such small-scale spatial variations are fully consistent with the accumulating evidence for the near ubiquity of subparsec-scale structure in interstellar clouds (e.g. Heiles 1997; Price, Crawford & Barlow 2000; Pan, Federman & Welty 2001).

All three stars have a strong, molecular component close to zero heliocentric velocity, which here we take to be the main absorption associated with the Lupus clouds. The column densities of this component are similar towards all three stars (Table 2), although there are small, but significant, variations in its velocity; most obviously, it is redshifted by $\approx 1.8 \text{ km s}^{-1}$ towards HD 152249 relative to HD 152235. This velocity difference is confirmed by the independently obtained molecular line data (Fig. 1). Thus, if this component is indeed associated with the Lupus complex, we find a velocity gradient of 1.8 km s^{-1} over the 0.4-pc separation of the two lines of sight.

In principle, we could combine the K I linewidths obtained here with the molecular linewidths obtained in earlier work to solve equation (1) to deduce T_k and v_t for the molecular components. However, whereas (for the reasons discussed in Section 4) we have good reasons to believe that K I and Na I trace the same interstellar material, we cannot safely make this assumption for the molecular components. Indeed, the invalidity of this assumption is most clearly illustrated by the strongest K I and CN components towards HD 152236. Both occur at the same velocity (Fig. 1), both probably sample outlying molecular gas of the Lupus complex, and both have well-defined velocity dispersions of $b(\text{K I}) = 0.91 \pm 0.03 \text{ km s}^{-1}$ (Table 2) and $b(\text{CN}) = 0.61 \pm 0.02 \text{ km s}^{-1}$ [obtained from a re-analysis of the data presented by Crawford (1995), using the VAPID routine for consistency]. As the CN molecule ($A = 26$) is a factor of 1.5 times *lighter* than the K atom, it cannot produce narrower lines than K I if the two species exist co-spatially. Thus, the very narrow CN lines at this velocity indicate that the CN arises in a cooler and/or less turbulent section of the line of sight than that dominating the K I absorption. This is as expected from the results of chemical models (e.g. Federman et al. 1994), which predict that CN will occur preferentially in the denser, most shielded, inner regions of dense cloud envelopes, while K I is likely to have a greater spatial extent.

6.3.2 More distant components

The velocity components in the range $-20 \leq v_{\text{helio}} \leq -6 \text{ km s}^{-1}$ are interpreted as arising in more distant clouds, i.e. beyond the Lupus complex but in the foreground to Sco OB1 itself. As discussed by Crawford (1992b), the extinction survey of Neckel & Klare (1980, their region 343/+1) shows a sharp rise in interstellar extinction in the distance range 700–1000 pc in this general direction, which seems likely to be caused by the clouds responsible for these velocity components.

6.4 The positive-velocity component

One star in the present sample, HD 152249, exhibits an absorption component at a velocity ($+19.3 \text{ km s}^{-1}$) significantly more positive than expected for galactic rotation over the 1900-pc line of sight. Although this is the only example in the present study, all

nine of the Sco OB1 stars observed by Crawford et al. (1989) were found to exhibit such positive-velocity components in Ca II. Corresponding Na I components were only observed in two cases, including this component towards HD 152248 (although similar redshifted Na I components were seen towards three additional stars close to Sco OB1 on the sky). These positive-velocity components were found to have low Na I/Ca II ratios (≤ 0.4), which were interpreted as being caused by the removal of Ca from, or the non-adsorption of Ca on to, grain surfaces.

Crawford et al. suggested that these positive-velocity, low-Na I/Ca II, components arise in warm ($T_k \approx 5000 \text{ K}$) intercloud material, which is masked at more negative velocities by the stronger absorptions arising in the foreground clouds and the shell components. However, while this remains a reasonable interpretation for the bulk of the relatively broad ($b \geq 3.0 \text{ km s}^{-1}$) Ca II components (which were undetected in Na I), it is no longer a plausible interpretation for well-defined narrow components such as this one towards HD 152249. We see from Table 3 that the velocity dispersion of this component ($b_{\text{Na}} = 0.81 \pm 0.32 \text{ km s}^{-1}$) corresponds to a rigorous temperature upper limit of 1770 K, and allowance for non-zero turbulence could reduce the temperature considerably. It thus seems that this narrow component [and the apparently similar one observed towards the Sco OB1 star HD 152270 by Crawford et al. (1989)] arises in a cool clump of material moving *towards* the Sco OB1 association. The most natural explanation would be an origin on the *far side* of an expanding interstellar shell somewhere in the foreground. Indeed, combining the Na I column density obtained here (Table 2) with the Ca II column density obtained by Crawford et al. (1989) yields the very low ratio of $N(\text{Na I})/N(\text{Ca II}) = 0.12 \pm 0.04$. This is even lower than the values found in the Sco OB1 shell components, and certainly suggests the removal of adsorbed Ca from grain surfaces through shock sputtering within a swept-up interstellar shell (although, as for the Sco OB1 shell components discussed in Section 6.2, the very low b -value argues against the presence of active shocks at the present epoch).

One possible location for this component might be the far side of one of the expanding shells known to surround the nearby ($D \approx 140 \text{ pc}$) Sco–Cen association. In his detailed study of the interstellar medium in the vicinity of Sco–Cen, de Geus (1992) identified three H I shells associated with this association, and the line of sight to Sco OB1 passes through the largest of these [the so-called ‘Upper-Centaurus Lupus’ (UCL) shell; cf. his table 1]. On the other hand, the predicted heliocentric radial velocity for the far side of this structure, based on the parameters given by de Geus (1992), is $+10 \pm 2 \text{ km s}^{-1}$, which is rather less than the measured velocity of this component. Alternatively, the ~ 1900 -pc line of sight to Sco OB1 may sample other expanding interstellar structures which could be responsible. Conceivably, this component could even arise within Sco OB1 itself if HD 152249 were somewhat more distant than the other stars.

7 CONCLUSIONS

We have obtained ultra-high-resolution ($R \approx 9 \times 10^5$) observations of interstellar Na I and K I absorption lines towards three members of the Sco OB1 association. These observations have enabled us to resolve the intrinsic linewidths of most of the identified velocity components (excluding those that are fully saturated in Na I). In turn, this has enabled us to place tighter constraints on the physical conditions prevailing in the various interstellar components present

along this very complex interstellar sightline. The principal conclusions are as follows.

(i) The velocity dispersions (b -values) of the various absorption components exhibit no noticeable dependence on velocity. Indeed, with few exceptions, the high negative-velocity ($-50 \lesssim v_{\text{helio}} \lesssim -20 \text{ km s}^{-1}$) Sco OB1 shell components are no broader than those attributed to foreground clouds, and therefore cannot be significantly hotter or more turbulent (Fig. 2). Indeed, one of the shell components (that at -35.95 km s^{-1} towards HD 152235) exhibits clearly resolved hyperfine structure in NaI (Fig. 1), implying a rigorous upper limit to the kinetic temperature of only 450 K.

(ii) While the low NaI/CaII ratios of the shell components reported in previous work (Crawford et al. 1989) are still most plausibly attributed to the removal of adsorbed Ca atoms from grain surfaces by shock sputtering, the low b -values are generally inconsistent with gas at the high post-shock temperatures expected ($\sim 10^4 \text{ K}$). A comparison of the post-shock cooling time with the Ca adsorption time-scale indicates that the shell components could indeed have been subject to shock processing in the past, but that they are likely to have cooled below the observed temperature upper limits without significant re-adsorption of Ca having yet occurred.

(iii) One possible exception to the above is the broad ($b = 8.16 \pm 0.60 \text{ km s}^{-1}$) -51.9 km s^{-1} NaI component towards HD 152236. At the resolution employed here, it is difficult to hide unresolved structure within such a broad component (Fig. 3). If such substructure is indeed absent, then this component may well arise in a hot and/or turbulent medium in which shocks are currently active.

(iv) At lower heliocentric velocities ($-20 \lesssim v_{\text{helio}} \lesssim +5 \text{ km s}^{-1}$), the unsaturated KI spectra clearly reveal the complex velocity structure within the range occupied by the fully saturated NaI absorption troughs (Fig. 1). These are interpreted as arising in foreground clouds along the ~ 1900 -pc line of sight to Sco OB1. Although traced at lower resolution in previous work, the present KI observations have revealed the presence of many more velocity components in this range than previously suspected. Moreover, the narrow linewidths of many of them, have placed quite stringent constraints on their thermal and turbulent properties (Table 3).

(v) The strongest low-velocity components (in the range $-6 \lesssim v_{\text{helio}} \lesssim +6 \text{ km s}^{-1}$) are interpreted as arising in outlying gas associated with the Lupus complex of molecular clouds at a distance of $\sim 150 \text{ pc}$. This is supported by both the radial velocities (see Murphy, Cohen & May 1986) and the detection of molecular (CH, CN) components at these velocities in previous work. It then follows that the differences in velocity structure and column densities between the observed stars imply spatial inhomogeneities on a scale of $\lesssim 1 \text{ pc}$. In particular, we find a velocity gradient of 1.8 km s^{-1} over the 0.4 -pc separation of the lines of sight to HD 152235 and 152249 at the distance of the Lupus clouds.

(vi) The origin of the relatively weak, but well-defined, positive-velocity ($+19.3 \text{ km s}^{-1}$) component towards HD 152249 remains problematical. Such positive velocities cannot be explained by galactic rotation in this direction, and the most likely explanation would be an origin in the far side of an expanding foreground shell (possibly one of those known to surround the nearby Sco-Cen association).

ACKNOWLEDGMENTS

I am indebted to I. D. Howarth for his work in developing the VAPID line-fitting routine, P. J. Storey for helpful conversations concerning the KI isotope shift, W. P. S. Meikle for correspondence on the $^{39}\text{K}/^{41}\text{K}$ isotope ratio in supernova ejecta and the referee for constructive comments on the original manuscript. I thank PATT for the award of telescope time and PPARC for an Advanced Fellowship. This research has made use of the SIMBAD data base, operated at CDS, Strasbourg.

REFERENCES

- Barlow M. J., 1978, MNRAS, 183, 417
 Barlow M. J., Silk J., 1977, ApJ, 211, L83
 Barlow M. J., Crawford I. A., Diego F., Dryburgh M., Fish A. C., Howarth I. D., Spyromilio J., Walker D. D., 1995, MNRAS, 272, 333
 Bendali N., Duong H. T., Vialle J. L., 1981, J. Phys. B., 14, 4231
 Cowie L. L., Songaila A., York D. G., 1979, ApJ, 230, 469
 Crawford I. A., 1989, MNRAS, 241, 575
 Crawford I. A., 1990, MNRAS, 244, 646
 Crawford I. A., 1992a, MNRAS, 259, 47
 Crawford I. A., 1992b, MNRAS, 254, 264
 Crawford I. A., 1995, MNRAS, 277, 458
 Crawford I. A., 2000, MNRAS, 317, 996
 Crawford I. A., Barlow M. J., Blades J. C., 1989, ApJ, 336, 212
 Crawford I. A., Howarth I. D., Ryder S. D., Stathakis R. A., 2000, MNRAS, 319, L1
 Dambis A. K., Mel'nik A. M., Rastorguev A. S., 2001, Astron. Lett., 27, 58
 de Geus E. J., 1992, A&A, 262, 258
 Diego F., 1993, Appl. Opt., 32, 6284
 Diego F. et al., 1995, MNRAS, 272, 323
 Federman S. R., Strom C. J., Lambert D. L., Cardelli J. A., Smith Joseph C. L., 1994, ApJ, 424, 772
 Fich M., Blitz L., Stark A. A., 1989, ApJ, 342, 272
 Heiles C., 1984, ApJS, 55, 585
 Heiles C., 1997, ApJ, 481, 193
 Howarth I. D., Murray J., Mills D., Berry D. S., 1998, Starlink User Note, 50.21
 Howarth I. D. et al., 2001, MNRAS, submitted
 Humphreys R. M., 1978, ApJS, 38, 309
 Iwamoto K., Brachwitz F., Nomoto K., Kishimoto N., Hideyuki U., Hix W. R., Thielemann F.-K., 1999, ApJS, 125, 439
 Laval A., 1972, A&A, 21, 271
 McKee C. F., Hollenbach D. J., 1980, ARA&A, 18, 219
 Morton D. C., 1991, ApJS, 77, 119
 Münch G., 1957, ApJ, 125, 42
 Murphy D. C., Cohen R., May J., 1986, A&A, 167, 234
 Neckel Th., Klare G., 1980, A&AS, 42, 251
 Normandeau M., Taylor A. R., Dewdney P. E., 1996, Nat, 380, 687
 Pan K., Federman S. R., Welty D. E., 2001, ApJ, 558, L105
 Péquignot D., Aldrovandi S. M. V., 1986, A&A, 161, 169
 Perry C. L., Hill G., Christodoulou D. M., 1991, A&AS, 90, 195
 Price R. J., Crawford I. A., Barlow M. J., 2000, MNRAS, 312, L43
 Price R. J., Crawford I. A., Barlow M. J., Howarth I. D., 2001, MNRAS, in press
 Raboud D., Cramer N., Bernasconi P. A., 1997, A&A, 325, 167
 Shorridge K. et al., 1998, Starlink User Note, 86.16
 Spitzer L., 1978, Physical Processes in the Interstellar Medium. Wiley, New York
 Struve O., 1944, ApJ, 100, 189
 van Genderen A. M., Bijleveld W., van Groningen E., 1984, A&AS, 58, 537
 Walborn N. R., 1982, ApJS, 48, 145
 Welty D. E., Hobbs L. M., 2001, ApJS, 133, 345
 Welty D. E., Hobbs L. M., Kulkarni V. P., 1994, ApJ, 436, 152

This paper has been typeset from a $\text{\TeX}/\text{\LaTeX}$ file prepared by the author.